Impact of Horizontal Diffusion on T21, T42, and T63 Singular Vectors

ROBERTO BUIZZA

European Centre for Medium-Range Weather Forecasts, Shinfield Park, Reading, United Kingdom

(Manuscript received 26 December 1995, in final form 15 July 1997)

ABSTRACT

The (linear) time evolution of singular vectors computed with a primitive equation model following a 36-h evolving trajectory is analyzed at horizontal triangular spectral truncations T21, T42, and T63.

First, for each resolution, the impact of horizontal diffusion on the singular vectors characteristics (amplification factors, total energy spectra) is analyzed. Forecast error and singular vectors computed with different horizontal diffusion damping times are compared to assess whether, at each resolution, forecast error projection onto the first 10 most unstable singular vectors is maximized for specific values. Results suggest that better projections are obtained with horizontal diffusion damping times on the smallest scale (on divergence) of 3 h at T42 and T63 resolution, and of 12 h at T21.

Then amplification factors, geographical locations, total energy vertical distributions, and spectra of T21, T42, and T63 singular vectors computed, respectively, with 12-, 3-, and 3-h damping time on the smallest scale are analyzed. The ratio among the singular vector amplification factors at T21:T42:T63 resolution is shown to be approximately 1:1.5:2.5. The geographical location and the total energy vertical distribution of T21, T42, and T63 singular vectors are quite similar. By contrast, total energy spectra differ substantially. Forecast error projection onto singular vectors is shown to be slightly larger if higher-resolution singular vectors are used. It is argued that the impact of horizontal resolution on the forecast error projection is marginal because of the lack of physical processes in the forward and adjoint tangent model versions. Moreover, the fact that forecast error projections onto the leading 10 singular vectors are rather small could be seen as an indication that more singular vectors are needed to capture the growing components of forecast error.

Finally, singular vectors and forecast errors are compared to quantify the relevance of the singular vectors of day *d* to capture the growing features of the error of the forecast started on day *d*. Results indicate that forecast error projection onto the leading 10 singular vectors decreases if singular vectors of a wrong date are used.

1. Introduction

Following analytical studies (Farrell 1982; Boyd 1983), singular vectors have been used to investigate perturbation growth in models with a small number of degrees of freedom (Lacarra and Talagrand 1988; Borges and Hartmann 1992; Molteni and Palmer 1993), and to study the finite time potential growth of perturbations in laboratory and geophysical flows (Farrell 1988a,b). More recently, singular vectors have been computed using more complex primitive equation models (Buizza et al. 1993).

The singular vector approach to the study of atmospheric instabilities has been related to other methods by Buizza and Palmer (1995), who have described, at least in some restrictive conditions, the relationship between singular vectors, eigenmodes, and Lyapunov vectors. The reader is also referred to Toth and Kalnay (1993) for a comparison of the characteristics of the singular vectors and of the so-called bred modes.

Singular vectors depend, by definition, on the choice of a metric (or inner product, and its associated norm) in the tangent space of the trajectory and on the optimization time interval over which growth is maximized.

Molteni et al. (1996) have compared singular vectors computed using a total energy and an enstrophy norm, with the total energy norm, enstrophy norm, and squared streamfunction norm of analysis difference fields. They concluded that, when the singular vectors are used to generate initial conditions for ensemble prediction, the total energy inner product seems to be the most appropriate. Their indications are further supported by the results of Palmer et al. (1998). Thus, total energy norm is used in this paper.

The sensitivity to the choice of optimization time interval has been studied at T21 truncation by Buizza (1994), who found similarity among singular vectors computed with optimization time intervals between 24 and 72 h. While 24 h can be considered, in our context, the lower bound on the possible choice of optimization time interval, the upper bound on the optimization time interval is fixed by the validity of the linear approxi-

Corresponding author address: Dr. Roberto Buizza, European Centre for Medium-Range Weather Forecasts, Shinfield Park, Reading, Berkshire RG2 9AX, United Kingdom.
E-mail: ner@ecmwf.int

mation. For perturbations computed at T21 and with initial amplitudes comparable with analysis error estimates, this time limit has been estimated to be of the order of 48 h (Buizza 1995). Since we are interested in comparing T21, T42, and T63 singular vectors, and since singular vectors with horizontal resolution higher than T21 are characterized by more rapid growth (Hartmann et al. 1995; Buizza et al. 1997), the optimization time interval is set to 36 h.

This work, which could be considered a continuation of the study by Hartmann et al. (1995), presents a more complete investigation on the impact of horizontal resolution on singular vectors' characteristics. In particular, some of the questions put forward by Hartmann et al. (1995) are addressed considering not only T21 and T42, but also T63 resolution.

Hartmann et al. (1995) compared T21 and T42 singular vectors growing over a 72-h time interval and computed with a horizontal diffusion damping time of 30 h at T42 and of 5 days at T21 on the smallest scale. Following this choice, they showed that T42 singular vectors have approximately double the T21 amplification rate. Applying a spectral truncation operator to the initial, to the optimization, or to both the initial and the optimization time, 1) they confirmed the upscale total energy transfer during the singular vector time evolution pointed out by Buizza and Palmer (1995); 2) they demonstrated that the optimization time structure of the singular vectors is insensitive to the presence or absence of large scales in the initial perturbation; 3) they showed that singular vectors constrained to be of large scale at initial time grow much more slowly than unconstrained perturbations and tend to be more barotropic in structure; 4) they concluded that ''It is of great fundamental interest for numerical weather prediction to determine whether linear growth rates continue to increase with resolution, and, if so, at what rate.'' The last question is one of the points discussed in this paper.

A limitation of the work of Hartmann et al. (1995) is that their results refer to singular vectors computed with specific horizontal diffusion damping times. Another of the points discussed in this paper is the sensitivity of singular vectors' characteristics, for example, amplification rate and total energy spectra, to changes in horizontal diffusion strength. Moreover, it is investigated whether, if singular vectors are used to sample forecast error growing directions, specific damping times should be used at each resolution.

This study is based on the analysis of 11 consecutive days. For each day, singular vectors growing over a 36-h time period have been computed at T21, T42, and T63 horizontal resolution, with horizontal diffusion damping times on the smallest scale (on divergence) ranging from 1.5 to 48 h. Due to computer limitations only the first 10 singular vectors are considered. [In terms of computer time with the European Centre for Medium-Range Weather Forecasts (ECMWF) CRAY C90 computer, it costs approximately 6 (28) times more to compute a T42 (T63) instead of a T21 singular vector.]

After this introduction, a brief overview of the singular vector definition and the definition of the inner product and the associated norm used to compare singular vectors are reported in section 2. In section 3, the synoptic situation is described. In section 4, the sensitivity of T21, T42, and T63 singular vectors to horizontal diffusion is analyzed. For each resolution, singular vectors' total energy spectra, and similarity indices between different growing subspaces (Buizza 1994) are computed. Moreover, following Buizza et al. (1997), forecast errors and singular vectors are compared to check whether higher forecast error projections onto unstable subspaces spanned by the leading 10 singular vectors could be obtained with specific damping times. In section 5, T21, T42, and T63 singular vectors computed with, respectively, 12-, 3-, and 3-h horizontal diffusion damping time are compared. First, the singular vector amplification factors, their geographical locations, and the total energy vertical distributions and spectra are compared. Then, it is investigated whether the similarity between T42 and T63 singular vectors is stronger than the similarity between T21 and T42 singular vectors. By modifying the weights of different spectral components when computing inner products, a detailed investigation is performed to highlight the scale of the major differences/similarities. Finally, conclusions are drawn in section 6.

2. Methodology

A brief description of the singular vector definition, and the methodology applied throughout this work is reported hereafter. The reader is referred to Buizza and Palmer (1995) for a more complete documentation.

a. Singular vector definition

Let $\mathbf{L}_P(t, t_0)$ be the integral propagator of the dynamical equations linearized about a nonlinear trajectory, $\overline{\mathbf{x}}(t)$,

$$\mathbf{x}'(t) = \mathbf{L}_P(t, t_0)\mathbf{x}'(t_0), \tag{1}$$

that maps a perturbation $\mathbf{x}'$ at initial time t_0 to optimization time t.

Let $\langle \ldots ; \ldots \rangle_N$ define the total energy inner product between two state vectors $\mathbf{x}$, $\mathbf{y}$

$$\langle \mathbf{x}; \mathbf{y} \rangle_N = \frac{1}{2} \int_0^1 \int_\Sigma \left(\nabla \Delta^{-1} \zeta_\mathbf{x} \cdot \nabla \Delta^{-1} \zeta_\mathbf{y} + \nabla \Delta^{-1} D_\mathbf{x} \cdot \nabla \Delta^{-1} D_\mathbf{y} + RT_r \ln \pi_\mathbf{x} \ln \pi_\mathbf{y} + \frac{C_p}{T_r} T_\mathbf{x} T_\mathbf{y} \right) d\sigma \left(\frac{\partial p}{\partial \eta} \right) d\eta, \tag{2}$$

computed in spectral space considering only the spectral components up to total wavenumber N, with ($\zeta_{\mathbf{x}}$, $D_{\mathbf{x}}$, $T_{\mathbf{x}}$, $\ln\pi_{\mathbf{x}}$) being the vorticity, divergence, temperature, and logarithm of surface pressure components of the state vector $\mathbf{x}$. Also, C_p is specific heat of dry air at constant pressure, $T_r = 300$ K, and y is the ECMWF hybrid vertical coordinate.

Let $\| \ldots \|_N$ be the norm associated with the inner product $\langle \ldots ; \ldots \rangle_N$

$$\|\mathbf{x}\|_N^2 = \langle \mathbf{x}; \mathbf{x} \rangle_N. \tag{3}$$

Let $\mathbf{L}_{\mathrm{P}}^*$ be the adjoint of $\mathbf{L}_{\mathrm{P}}$ with respect to the total energy inner product $\langle \ldots ; \ldots \rangle_N$. From Eqs. (1)–(3) it follows that the total energy of a perturbation $\mathbf{x}'$ at time t is

$$\|\mathbf{x}'(t)\|_N^2 = \langle \mathbf{x}'(t_0); \mathbf{L}_{\mathrm{P}}^* \mathbf{L}_{\mathrm{P}} \mathbf{x}'(t_0) \rangle_N. \tag{4}$$

Let $\mathbf{T}$ be a local projection operator (Buizza and Palmer 1995), defined as

$$\mathbf{T} = \mathbf{S}^{-1} \mathbf{G} \mathbf{S}, \tag{5}$$

where $\mathbf{S}$ is a spectral to gridpoint transformation, and $\mathbf{G}\mathbf{x}_{\mathrm{G}}$ denotes the multiplication of a vector, $\mathbf{x}_{\mathrm{G}}$, defined in physical space by the hat function

$$g(\mathbf{p}) = 1 \quad \text{if} \quad \mathbf{p} \in \Sigma, \tag{6a}$$

$$g(\mathbf{p}) = 0 \quad \text{if} \quad \mathbf{p} \notin \Sigma, \tag{6b}$$

where $\mathbf{p}$ defines the coordinates of a grid point and X is a geographical region. The norm of perturbations located at optimization time over the Northern Hemisphere extratropics can be computed by applying the operator $\mathbf{T}$ with

$$\mathrm{X} = \{ \mathbf{x}_{\mathrm{G}} \quad \text{if} \quad \mathrm{lat}(\mathbf{x}_{\mathrm{G}}) \geq 30^{\circ}\mathrm{N} \}, \tag{7}$$

as

$$\|\mathbf{x}'(t)\|_N^2 = \langle \mathbf{x}'(t_0); \mathbf{L}_{\mathrm{P}}^* \mathbf{T}^2 \mathbf{L}_{\mathrm{P}} \mathbf{x}'(t_0) \rangle_N. \tag{8}$$

Let $\mathbf{W}_0$ be a spectral truncation operator [Hartmann et al. 1995, Eqs. (12)–(13)], so that $\mathbf{W}_0\mathbf{x}$ denotes the multiplication of each spectral component of the vector $\mathbf{x}$ by the following function $w(n, m)$ in wavenumber space:

$$w(n, m) = 1 \quad \text{if} \quad (n, m) \in \Omega, \tag{9a}$$

$$w(n, m) = 0 \quad \text{if} \quad (n, m) \notin \Omega, \tag{9b}$$

where n is the total wavenumber, m is the zonal wavenumber, and Ω a spectral space subspace. The norm of perturbations that, at initial time, have only spectral components belonging to the spectral space region Ω can be computed applying $\mathbf{W}_0$

$$\|\mathbf{x}'(t)\|_N^2 = \langle \mathbf{x}'(t_0); \mathbf{W}_0^* \mathbf{L}_{\mathrm{P}}^* \mathbf{L}_{\mathrm{P}} \mathbf{W}_0 \mathbf{x}'(t_0) \rangle_N. \tag{10}$$

Thus, perturbations with Northern Hemisphere maximum growth over the optimization time interval $t - t_0$, which at initial time have spectral components belonging to the spectral space region Ω, are the solutions of the eigenvalue problem

$$\mathbf{W}_0^* \mathbf{L}_{\mathrm{P}}^* \mathbf{T}^2 \mathbf{L}_{\mathrm{P}} \mathbf{W}_0 \mathbf{v}_j = \sigma_j^2 \mathbf{v}_j. \tag{11}$$

The eigenvectors $\mathbf{v}_j$ form a complete orthogonal basis in the M-dimensional tangent space of linear perturbations (Noble and Daniel 1977). The eigenvalues σ_j are called the singular values, and the eigenvectors $\mathbf{v}_j$ the (right) singular vectors of the operator $\mathbf{T}\mathbf{L}_{\mathrm{P}}\mathbf{W}_0$. The singular vectors are ranked with respect to the amplification rate (jth subscript), have unit norm at initial time, and have optimization time norm equal to the corresponding singular values.

Singular vectors computed at different resolution, for consecutive days, and evolved for different time periods t are compared in this paper. Hence, for ease of comparison, new unit vectors are defined for each time t, as follows.

Consider the jth singular vector $\mathbf{v}_j(t)$ computed at resolution Tn (where n is 21, 42, or 63), for day d, evolved at time t, and normalized. Introduce two superscripts in the singular vector notation, and define a new vector, $\tilde{\mathbf{v}}_j^{d,\mathrm{T}n}(t)$, as

$$\tilde{\mathbf{v}}_j^{d,\mathrm{T}n}(t) \equiv \frac{\mathbf{v}_j(t)}{\|\mathbf{v}_j(t)\|}. \tag{12}$$

Note that the singular vectors are orthogonal at initial and optimization time, that is, in our case at $t = 36$ h, while they lose orthogonality at other times. Thus, for times $t \neq 0$, 36 h, a new set of orthonormal vectors is computed from $\tilde{\mathbf{v}}_j^{d,\mathrm{T}n}(t)$ applying a Graam–Schmidt reorthogonalization algorithm,

$$\mathbf{v}_j^{d,\mathrm{T}n}(t) \equiv \tilde{\mathbf{v}}_j^{d,\mathrm{T}n}(t) - \sum_{k=1}^{j-1} \langle \tilde{\mathbf{v}}_j^{d,\mathrm{T}n}(t); \mathbf{v}_k^{d,\mathrm{T}n}(t) \rangle \, \mathbf{v}_k^{d,\mathrm{T}n}(t)$$

$$\text{for} \quad j = 1, 10. \tag{13}$$

Hereafter, when discussing singular vectors for times $t \neq 0$, 36 h we will always refer to these vectors. (In practice, the loss of orthogonality for times $t \leq 48$ h is very small.)

b. Growing subspace and similarity index definition

Let $\mathbf{P}^{d,\mathrm{T}n}(t)$ be the 10-dimensional subspace of the phase space of the system spanned by the first 10 fastest growing singular vectors $\mathbf{v}_j^{d,\mathrm{T}n}(t)$ computed for day d, at truncation Tn, evolved to time t,

$$\mathbf{P}^{d,\mathrm{T}n}(t) = \{ \mathbf{v}_j^{d,\mathrm{T}n}(t), j = 1, 10 \}. \tag{14}$$

Consider two singular vectors $\mathbf{v}_j^{d,\mathrm{T}n}(t)$ and $\mathbf{v}_k^{d,\mathrm{T}m}(t)$ of the same day d but computed at different resolutions. We can determine the similarity of their components up to total wavenumber N, with $N \leq \min(n, m)$, by computing the squared inner product

$$\langle \mathbf{v}_j^{d,\mathrm{T}n}(t); \mathbf{v}_k^{d,\mathrm{T}m}(t) \rangle_N^2. \tag{15}$$

Similarly, the jth singular vector $\mathbf{v}_j^{d,\mathrm{T}n}(t)$ of day d, at resolution Tn, at time t, can be compared with the kth

singular vector $\mathbf{v}_k^{d',\mathrm{T}m}(t')$, of day d', at resolution Tm, at time t', by computing the squared inner product

$$\langle \mathbf{v}_j^{d,\mathrm{T}n}(t);\, \mathbf{v}_k^{d',\mathrm{T}m}(t')\rangle_N^2, \tag{16}$$

where $d + t = d' + t'$, so that the two singular vectors are compared at the same verification time, and $N \leq \min(n, m)$.

The similarity index of two growing subspaces, $\mathbf{P}^{d,\mathrm{T}n}(t)$ and $\mathbf{P}^{d',\mathrm{T}m}(t')$, can be defined as

$$s[\mathbf{P}^{d,\mathrm{T}n}(t),\, \mathbf{P}^{d',\mathrm{T}m}(t');\, N] \equiv \frac{1}{10}\sum_{j,k=1}^{10} \langle \mathbf{v}_j^{d,\mathrm{T}n}(t);\, \mathbf{v}_k^{d',\mathrm{T}m}(t')\rangle_N^2. \tag{17}$$

Note that $s[\mathbf{P}^{d,\mathrm{T}n}(t), \mathbf{P}^{d',\mathrm{T}m}(t'); N]$ is function of the truncation parameters Tn, Tm, and N, and of the time parameters d, d', t, and t'.

c. Forecast error and singular vectors

Consider a forecast error field,

$$\mathbf{e}_\rho^{d,\mathrm{T}n}(t) \equiv \overline{\mathbf{x}}^{d,\mathrm{T}n}(t) - \overline{\mathbf{x}}^{d+t,\mathrm{T}n}(0), \tag{18}$$

defined as the difference between the trajectory $\overline{\mathbf{x}}^{d,\mathrm{T}n}(t)$ started at day d and evolved at time t, and the corresponding analysis identified by $\overline{\mathbf{x}}^{d+t,\mathrm{T}n}(0)$, north of n (this geographical localization is applied since the singular vectors are defined to grow north of n).

The forecast error can be projected onto the growing subspace $\mathbf{P}^{d,\mathrm{T}n}(t)$, defined by the first 10 singular vectors of day d, computed at resolution Tn, and evolved to time t, thus defining the projected forecast error field

$$\tilde{\mathbf{e}}_\mathrm{f}^{d,\mathrm{T}n}(t) \equiv \sum_{k=1}^{10} \langle \mathbf{e}_\mathrm{f}^{d,\mathrm{T}n}(t);\, \mathbf{v}_k^{d,\mathrm{T}n}(t)\rangle_N \mathbf{v}_k^{d,\mathrm{T}n}(t). \tag{19}$$

The ratio between the total energy norms of the true and the projected forecast error field,

$$\mathrm{PI}_N^{d,\mathrm{T}n}(t) \equiv \frac{\|\tilde{\mathbf{e}}_\mathrm{f}^{d,\mathrm{T}n}(t)\|_N}{\|\mathbf{e}_\mathrm{f}^{d,\mathrm{T}n}(t)\|_N}, \tag{20}$$

can be used to measure the capability of the singular vectors to describe the growing part of forecast errors. This ratio is called the ''projection index.''

3. Synoptic situation and trajectories evaluation

The period analyzed in this paper starts on 3 September and ends on 13 September 1993. During the last days of this period, a type-B development (Petterssen and Smebye 1971) led to a very intense cyclone that affected the south of England. It was associated with the interaction of three systems, a midtropospheric disturbance moving from northwest to southeast, a low-level cyclone travelling eastward over the Atlantic ocean, and an almost stationary cyclone located over England itself.

Figure 1 shows the 1000- and 500-hPa geopotential height at 1200 UTC of 4, 8, and 12 September 1993. For the Pacific sector, on 4 September the circulation is characterized by a trough on the western side, with a developing cutoff low splitting the flow on the eastern side (Fig. 1a). During the next days, the trough deepens, and a deep cutoff low develops over the eastern Pacific (Fig. 1c). In the western Pacific, a cyclone develops during 9 and 10 September and decays afterward travelling eastward (Fig. 1e).

The North American sector is characterized by an almost stationary large-scale trough during the whole period. By contrast, the Atlantic–European region has rapid developments. On 4 September, a deep cyclone is located over the central Atlantic, while an area of high pressure affects the British Isles (Figs. 1a,b). During the next days this cyclone moves slowly eastward, and on 8 September is positioned southwest of England (Figs. 1b,c). On 8 September, a small-scale low-level cyclone associated with an intensifying upper-level trough starts developing in the northwestern Atlantic. At the same time, a low-level small-scale disturbance starts travelling from the northeastern coast of America toward Europe (this can be related to the remains of Tropical Cyclone Floyd). Two days later, the NW–SE-travelling system is located approximately at (20°W, 60°N), and the disturbance travelling from the east cost of America is at approximately (45°W, 45°N) (not shown). This latter disturbance, in particular, intensifies very strongly during the following two days. On 12 September, these two travelling systems meet the stationary cyclone located south of England, and the situation rapidly evolves into a very intense cyclone (Figs. 1e,f).

Since singular vectors are computed following a time-evolving trajectory (calculated at the same resolution as the singular vectors), they are affected by trajectory accuracy. Generally speaking, the forecast error of trajectories computed at higher resolution is about 35% smaller than the forecast error of T21 trajectories. Considering the components with total wavenumber $0 \leq n \leq 21$, while a large reduction of the error (30%) is obtained by increasing the resolution from T21 to T42, a small improvement is achieved by a further resolution increase to T63. The small impact of the resolution increase from T42 to T63 can be detected also when considering the components with total wavenumber $21 \leq n \leq 42$ (a 10% reduction is obtained by increasing the resolution from T42 to T63). In addition to this, trajectories have been compared to quantify their relative difference. Considering wavenumbers $0 \leq n \leq 21$, the distance of a T21 trajectory from either a T42 or a T63 trajectory is 3–4 times larger than the distance between a T42 and a T63 trajectory, while the difference between the T42 and the T63 trajectories is very small, indicating that these components are already well defined at T42.

4. Impact of horizontal diffusion on singular vectors

Horizontal diffusion is not a dominant process in numerical weather prediction models, since many diabatic

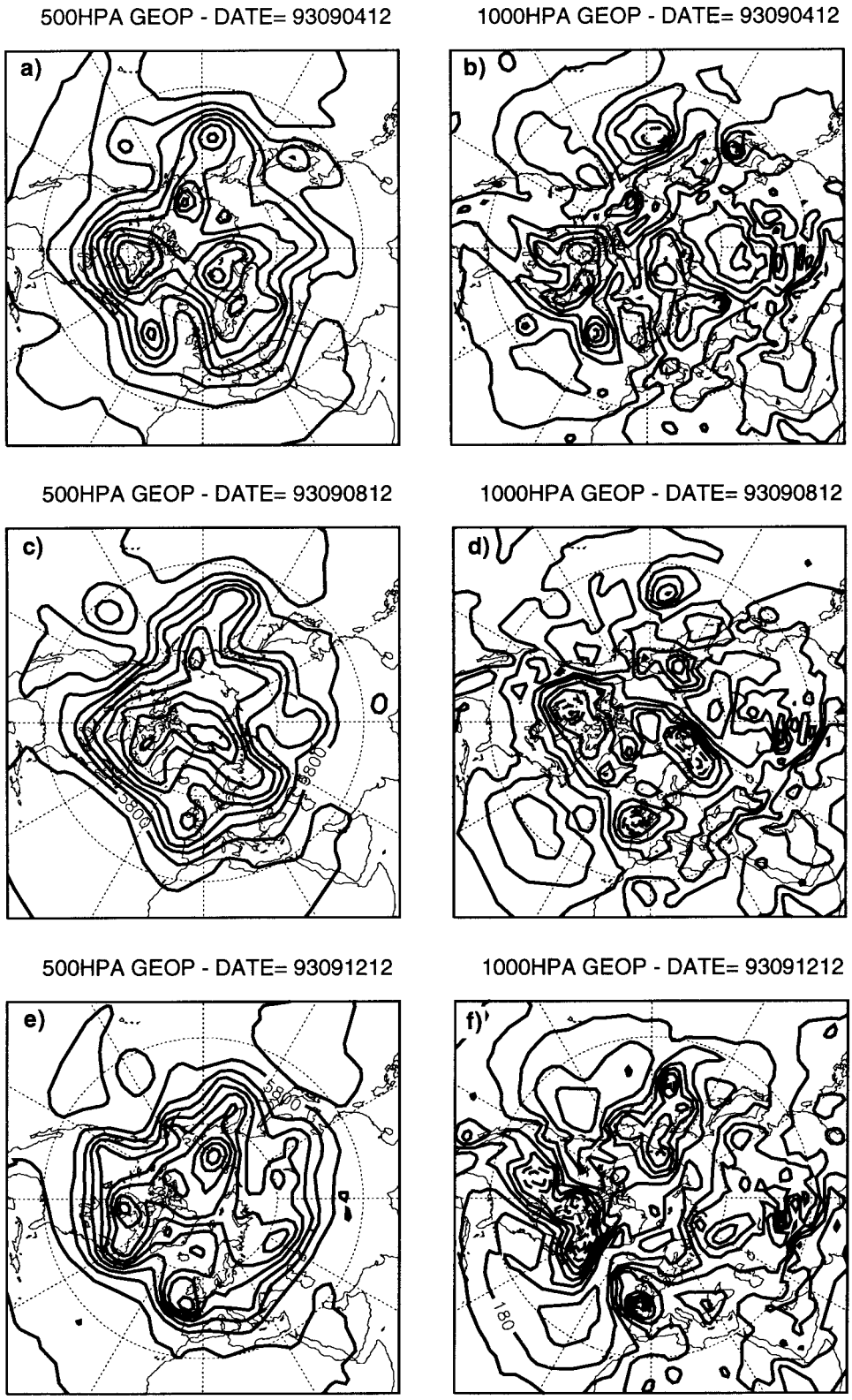

FIG. 1. (a) 500-hPa geopotential height field and (b) 1000-hPa geopotential height field for 4 September 1993. (c), (d): As (a), (b) but for 8 September. (e), (f): as (a), (b) but for 12 September. Contour isolines (a), (c), (e) 80 m and (b), (d), (f) 40 m.

TABLE 1. Experiments naming convention as a function of horizontal resolution Tnn and horizontal diffusion damping time (in hours).

Experiment name	Damping time on divergence
Tnn_1.5	1.5 h
Tnn_3	3 h
Tnn_6	6 h
Tnn_12	12 h
Tnn_24	24 h
Tnn_48	48 h

processes are parameterized, but it has an important role in the forward and adjoint tangent model versions, where the only diabatic parameterized process is, up to now, vertical diffusion and surface drag. In numerical weather prediction, horizontal diffusion is a numerical artifact used to control the noise of the model and to allow longer time steps to be used. It is a process that is revised continuously as models evolve. Horizontal diffusion damping times, on the smallest scale, are usually defined by experience, and for the ECMWF numerical weather prediction model, for example, they range from 45 min at T213 resolution to 48 h at T63 resolution (on divergence).

The first aim of this section is to quantify the impact of horizontal diffusion on singular vectors' characteristics, while the second is to investigate whether, when the singular vectors are used for predictability studies, certain choices of damping times should be made.

For each day and for each horizontal resolution, singular vectors have been computed with horizontal diffusion damping times on divergence ranging from 1.5 to 48 h on the smallest scale (Table 1). The horizontal diffusion is a ∇^4 scheme, with damping times on vorticity and temperature that are 2.5 times longer than that applied to divergence. Thus, given a certain damping time $\tau_{\text{hdiff}}(N)$ on the smallest scale N, the damping time applied to a scale with total wavenumber n is approximately $\tau_{\text{hdiff}}(n) \sim (1/n^2)\tau_{\text{hdiff}}(N)$.

Apart from horizontal diffusion, the main characteristics of the singular vectors computation are

- 36-h optimization time interval;
- 19 vertical levels;
- T21, T42, or T63 horizontal spectral truncation;
- total energy norm [Eq. (3)];
- initialization procedure applied to the first five gravest modes (see Buizza et al. 1993);
- linear and adjoint integration following a time-evolving trajectory;
- trajectory integration using the full ECMWF physics, forward, and adjoint linear integrations using a linear vertical diffusion and surface drag scheme (Buizza 1994);
- local projection operator (Buizza and Palmer 1995) to confine the growth in the Northern Hemisphere extratropics ($\phi \geq 30°$N).

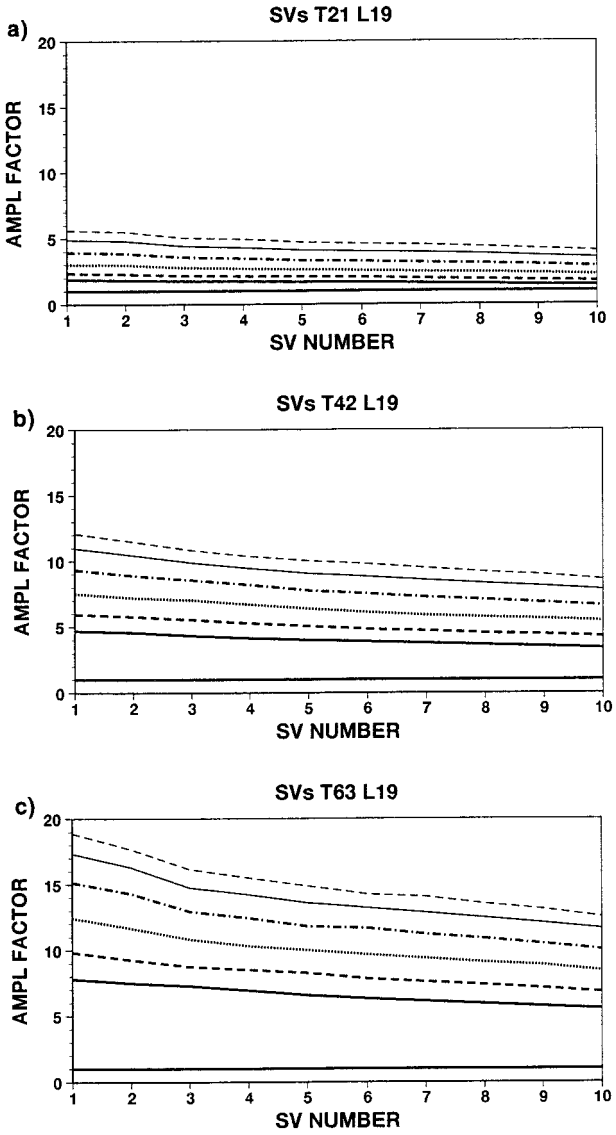

FIG. 2. Mean amplification factor of the first 10 most unstable singular vectors computed at (a) T63, (b) T42, and (c) T21 horizontal resolution, and with a horizontal diffusion damping time of 1.5 (solid), 3 (dashed), 6 (dotted), 12 (chain dash), 24 (thin solid), and 48 (thin dashed) hours on the smallest scale (on divergence).

a. Amplification factor

Figure 2 shows the mean amplification factors (computed averaging the amplification factors relative to the 11 consecutive initial dates) of the first 10 most unstable singular vectors as a function of (horizontal) resolution and of (horizontal diffusion) damping time.

The impact of horizontal diffusion is stronger when the resolution is higher. Considering, for example, T63 singular vectors (Fig. 2c), the mean amplification factor of the fastest growing singular vector increases from, say, 5 to 19 when the damping time is increased from 1.5 to 48 h.

Considering singular vectors computed with the same

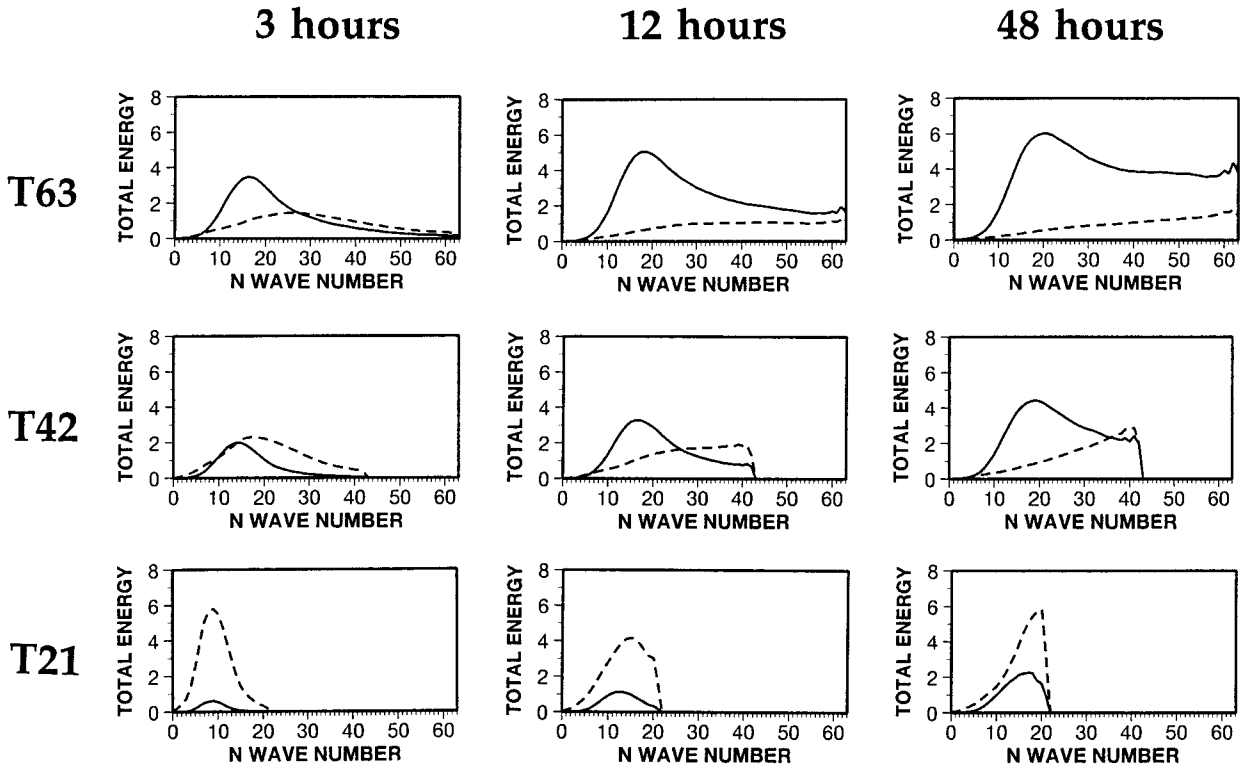

FIG. 3. Mean total energy spectrum (averaged using the first 10 most unstable singular vectors) of T63, T42, and T21 singular vectors computed with horizontal diffusion damping times of 3, 12, and 48 h.

TABLE 2. Impact of horizontal damping time on the similarity index (in percentage) between unstable subspaces. Standard deviations reported in parentheses.

(a) T63 singular vectors computed with a T63 norm truncation.

T63 proj	T63_3	T63_6	T63_12	T63_24	T63_48
T63_1.5	75.4 (3.5)	56.1 (2.8)	41.2 (2.4)	32.7 (2.4)	28.6 (3.8)
T63_3	—	75.1 (3.8)	61.6 (3.8)	50.5 (4.6)	45.3 (6.1)
T63_6		—	77.6 (4.9)	69.4 (6.1)	63.6 (7.0)
T63_12			—	81.5 (4.8)	76.2 (4.3)
T63_24				—	83.4 (4.9)

(b) T42 singular vectors computed with a T42 norm truncation.

T42 proj	T42_3	T42_6	T42_12	T42_24	T42_48
T42_1.5	72.8 (3.5)	51.6 (3.1)	33.5 (2.8)	23.4 (2.5)	18.2 (1.3)
T42_3	—	73.0 (4.7)	53.8 (4.0)	41.4 (3.0)	34.1 (2.9)
T42_6		—	75.3 (5.0)	62.5 (3.8)	54.5 (5.8)
T42_12			—	81.1 (6.1)	72.8 (6.2)
T42_24				—	85.6 (4.2)

(c) T21 singular vectors computed with a T21 norm truncation.

T21 proj	T21_3	T21_6	T21_12	T21_24	T21_48
T21_1.5	70.4 (2.9)	42.4 (2.1)	21.7 (2.8)	11.1 (2.2)	7.6 (1.9)
T21_3	—	70.9 (3.1)	44.1 (3.1)	26.6 (2.5)	19.5 (2.1)
T21_6		—	70.4 (4.2)	51.6 (3.7)	41.5 (2.9)
T21_12			—	75.1 (6.1)	66.9 (5.4)
T21_24				—	86.0 (5.0)

damping time, the amplification factor of the fastest growing singular vector increases from around 2 to 8 for a 1.5-h damping time, and from around 5.5 to 19 for a 48-h damping time when the resolution is increased from T21 to T63. Generally speaking, results show that the singular values spectra are flatter at T21 than at T63 resolution.

b. Total energy spectrum

Figure 3 shows the impact of resolution and damping time on mean total energy spectra (where the average is taken considering the first 10 singular vectors relative to the 11 consecutive initial dates). For any resolution, results indicate that the choice of damping time affects the spectra both at initial and final time, and that this effect is stronger at lower resolution. (Further discussion on the singular vectors' spectra is reported below in section 4d.)

c. Similarity of unstable subspaces

Table 2 reports, for each resolution, the impact of horizontal diffusion on the mean similarity index between unstable subspaces [computed averaging the similarity indices defined in Eq. (17) relative to the 11 different initial dates]. Considering two unstable subspaces computed with damping times τ_1 and τ_2, the

more the two damping times differ, the least similar are the unstable subspaces. The poor similarity, at any resolution *nn*, between experiments T*nn*_1.5 and T*nn*_48 reflects the very different total energy spectra of the relative singular vectors (Fig. 3). The fact that, at any resolution *nn*, the similarity index between experiments T*nn*_24 and T*nn*_48 is the largest suggests that a further enhancement of the damping time should have a very weak effect. This should be particularly true for T21 resolution.

d. Forecast error projection index

The results of Figs. 2–3 and Table 2 indicate a strong dependence of the singular vectors' characteristics from the choice of horizontal diffusion damping time. Is there a way to define, for each resolution, which damping time should be used when computing singular vectors?

The answer to this question is linked to the problem to which the singular vectors are applied. In our case, let us restrict the use of the singular vector to predictability studies, more precisely to estimate the directions along which forecast error grows fastest. In this context, the question could be answered by comparing singular vectors at optimization time (i.e., +36 h) with the error of +36-h forecasts, where the forecast error is defined as the error of the high-resolution T213L31 ECMWF operational model.

Figure 4a shows the mean projection index [as defined in Eq. (20), averaging the projection indices relative to the 11 different initial dates] computed for T63 (solid), T42 (dashed), and T21 (dotted) singular vectors considering only total wavenumbers $0 \leq n \leq 21$ [i.e., with $N = 21$ in Eq. (20)], as a function of the horizontal diffusion damping time. Regarding these scales, Fig. 4a shows that higher projection indices are obtained at T42 resolution with strong horizontal diffusion. By contrast, considering T21 singular vectors, the best result is obtained with a damping time of 12 h.

Since the use of a high horizontal resolution is aimed to also describe scales with total wavenumber $n \geq 21$, projection indices have been computed considering total wavenumbers $0 \leq n \leq 42$ for T42 and T63 singular vectors (Fig. 4b), and considering $0 \leq n \leq 63$ for T63 singular vectors (Fig. 4c). Figures 4b,c show that, when scales with $n \geq 21$ are considered, better results are obtained with damping times of 3 h for T42 singular vectors and of either 1.5 or 3 h for T63 singular vectors.

These results are reflected by the comparison of the mean forecast error total energy spectra (computed averaging the forecast errors relative to the 11 different initial dates, Fig. 5), with the total energy spectra at optimization time of the singular vectors (Fig. 3). In fact, for T21 singular vectors a weak horizontal diffusion is needed to have energy also on scales with wavenumber around $n \sim 21$, while for T42 or T63 singular vectors a strong horizontal diffusion is needed to avoid having too much energy in the far end of the spectrum.

Although we recognize that at T42 and T63 differences are small, we argue that these results indicate that, to have a larger projection of forecast error onto the unstable subspace spanned by the leading 10 singular vectors, a horizontal diffusion damping time on the smallest scale (on divergence) of 12 h should be used when computing T21 singular vectors, and that a 3-h damping time should be used at T42 and T63 resolution.

5. Comparison between T21, T42, and T63 singular vectors

Following the results presented in section 4, hereafter we will concentrate on experiments T21_12, T42_3, and T63_3 (Table 1), that is, on singular vectors computed at T21 with a 12-h damping time, and at T42 and at T63 with a 3-h damping time. These singular vectors will be simply referred to as T21, T42, and T63 singular vectors.

For completeness of comparison, singular vectors computed for each day from 4 to 11 September 1993 have been linearly evolved up to 48 h, and growing subspaces $\mathbf{P}^{d,\mathrm{T}n}(t)$, for $t = 12, 24, 36, 48$ h have been defined following Eqs. (13)–(14).

a. Amplification factor and geographical location

Figure 6 shows the ratio between the average amplification rate of T63 and T21 (solid), T42 and T21 (dashed), and T63 and T42 (dot) singular vectors. The average amplification rate increases approximately by a factor of 1.5 when going from T21 to T42, and by slightly more when further increasing the horizontal resolution to T63.

The contribution of different scales to the total energy growth can be assessed by comparing the amplification factor of unconstrained singular vectors with the amplification factor of singular vectors computed applying a spectral truncation operator on some components. Considering, for example, the fastest growing singular vector, at T21 resolution, the first and the second half of the total wavenumber space contribute almost equally to the singular vector growth, while at T42 resolution the contribution coming from the second half of the total energy spectrum (i.e., from the scales with total wavenumber $21 \leq n \leq 42$) is half the contribution coming from the first half of the spectrum. By contrast, at T63 resolution the scales with total wavenumber $42 \leq n \leq 63$ contribute only to 11% of the total growth. The comparison between the similarity indices of growing subspaces generated using the first 10 unconstrained and constrained singular vectors confirms that the contribution of scales with total wavenumber $42 \leq n \leq 63$ to the definition of T63 singular vectors is very small.

The geographical distributions of the T21, T42, and T63 singular vectors (where the location of each singular vector has been defined as the geographical point with maximum vorticity square, Fig. 7) are quite similar,

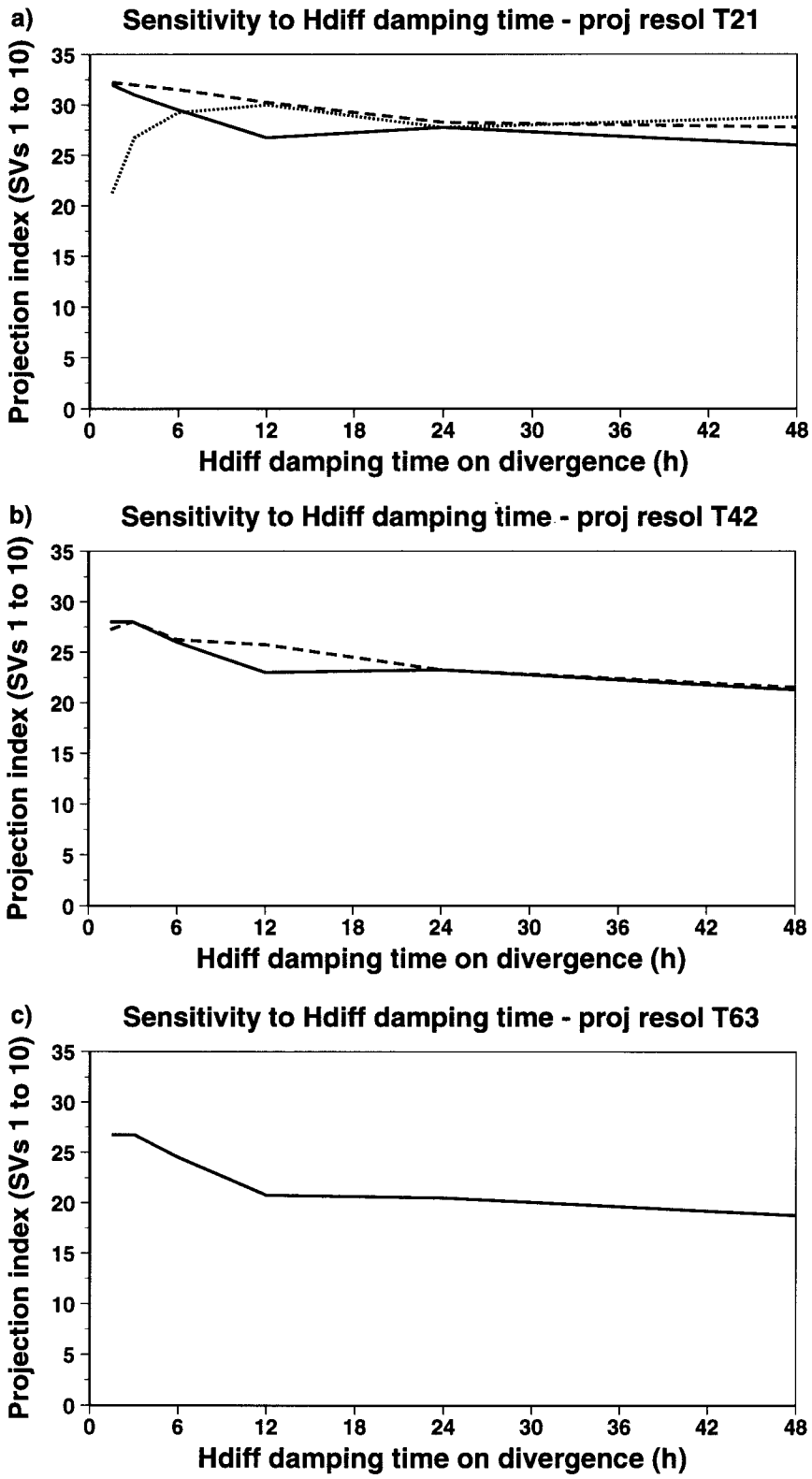

FIG. 4. Mean projection index as a function of horizontal diffusion damping times, computed considering scales with total wavenumber (a) $0 \leq n \leq 21$, (b) $0 \leq n \leq 42$, (c) $0 \leq n \leq 63$, relative to T63 (solid), T42 (dashed), and T21 (dotted) singular vectors. Standard deviation values range between 3.6 and 5.

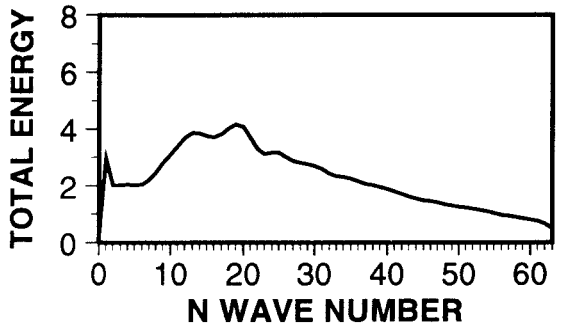

FIG. 5. Mean total energy spectrum (averaged considering the 11 different starting dates) of the error of the +36-h T213L31 forecast.

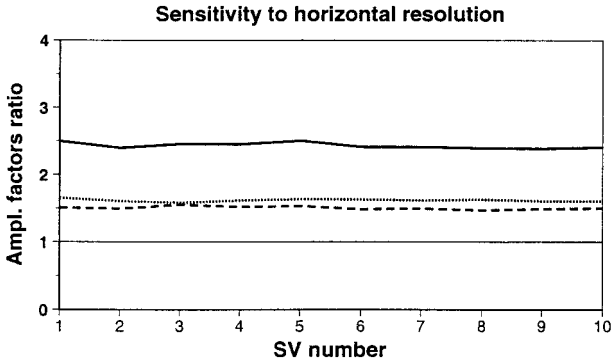

FIG. 6. Ratio between the average amplification factor of T63_3 and T21_12 (solid), T42_3 and T21_12 (dashed), and T63_3 and T42_3 singular vectors.

although some differences can be detected. For example, more singular vectors are growing in the European region at T42 or T63, rather than at T21 resolution.

b. Total energy vertical distribution and spectrum

Figure 8 shows the time evolution of the average total energy vertical distribution as a function of the model level (left panels), and the time evolution of the total energy spectrum as a function of the total wavenumber (right panels).

The T21, T42, and T63 total energy vertical distributions are very similar, peaking at about model level 13 (approximately 700 hPa) at initial time and at about model level 9 at optimization time (approximately 300 hPa). The perturbation growth can be qualitatively understood in terms of wave-action concepts (Buizza and Palmer 1995). Specifically, the conservation of wave action for a perturbation initially located close to the baroclinic steering level and vertically propagating toward the jet level, implies energy growth. Such a process has been modeled in a WKBJ approximation by Zeng (1983).

Considering the total energy spectra, Fig. 8 shows that (with our choice of a 12-h damping time on the smallest scale) the T21 truncation limit is very close to the total energy maximum. The upscale total energy transfer during the time evolution described by Buizza and Palmer (1995) is more evident in the T42 and T63 spectra. At both these resolutions, the maximum of the total energy spectrum shifts from total wavenumber 20–25 to around total wavenumber 14 at optimization time (bold solid line). For each forecast time, Fig. 8 shows that the average total energy spectrum shifts more to the left if resolution is increased. For example, at optimization time, the spectrum peaks at total wavenumber $n \approx 12$ at T21, $n \approx 14$ at T42, and $n \approx 16$ at T63.

c. Similarity of unstable subspaces

First, we compare growing subspace computed for the same day but at different resolution (question Q1). Then, we discuss whether one could approximate the growing subspace of day $d + 1$ by using the growing subspace of day d, or even day $d - 1$. In particular, we compare growing subspaces computed for different days and evolved for the same time [i.e., $d \neq d'$, $t = t'$ in Eq. (17), question Q2], or growing subspaces computed for different days but evolved for different times so that they verify at the same time [i.e., $d \neq d'$, $t \neq t'$, $d + t = d' + t'$ in Eq. (17), question Q3]. Figure 9 is a schematic of these two comparisons: two trajectories **A** and **B** are sketched with their growing subspaces at different forecast times. To answer to question Q2, the similarity between the growing subspaces of **A** and **B** at initial time $t = 0$ [$\mathbf{P}^{\mathbf{A}}(t = 0)$ and $\mathbf{P}^{\mathbf{B}}(t = 0)$] and at optimization time $t = 36$ h [$\mathbf{P}^{\mathbf{A}}(t = 36$ h) and $\mathbf{P}^{\mathbf{B}}(t = 36$ h)] is discussed. To answer to question Q3, the similarity of growing subspaces evolved to the same verifying time [e.g., $\mathbf{P}^{\mathbf{A}}(t = 36$ h) and $\mathbf{P}^{\mathbf{B}}(t = 12$ h)] is discussed.

> Q1. *How similar are the growing subspaces* $\mathbf{P}^{d,\mathrm{T21}}(t)$, $\mathbf{P}^{d,\mathrm{T42}}(t)$, $\mathbf{P}^{d,\mathrm{T63}}(t)$ *at initial and optimization times* ($t = 0$, 36 h)?

Table 3 lists the average similarity indices, computed considering $\mathbf{P}^{d,\mathrm{T21}}(t)$, $\mathbf{P}^{d,\mathrm{T42}}(t)$, $\mathbf{P}^{d,\mathrm{T63}}(t)$. The growing subspaces are more similar at optimization than at initial time because the total energy projects on fewer wavenumbers at optimization than at initial time (see Fig. 8). The similarity between T42 and T63 growing subspaces is stronger than the similarity between T21 and either T42 or T63 growing subspaces.

> Q2. *How similar are growing subspaces computed for successive days at initial and optimization times* ($t = 0$, 36 h)? *More precisely, how similar are* $\mathbf{P}^{d,\mathrm{Tn}}(t)$, $\mathbf{P}^{d',\mathrm{Tn}}(t)$, *for* $d' = d + 24$ h *or* $d' = d + 48$ h? *Does the similarity depend on the resolution* Tn?

Table 4 lists the average similarity indices computed between growing subspaces 1 or 2 days apart, at optimization time $t = 36$ h (at initial time, similarity indices at T21 are about 10% smaller, while at T42

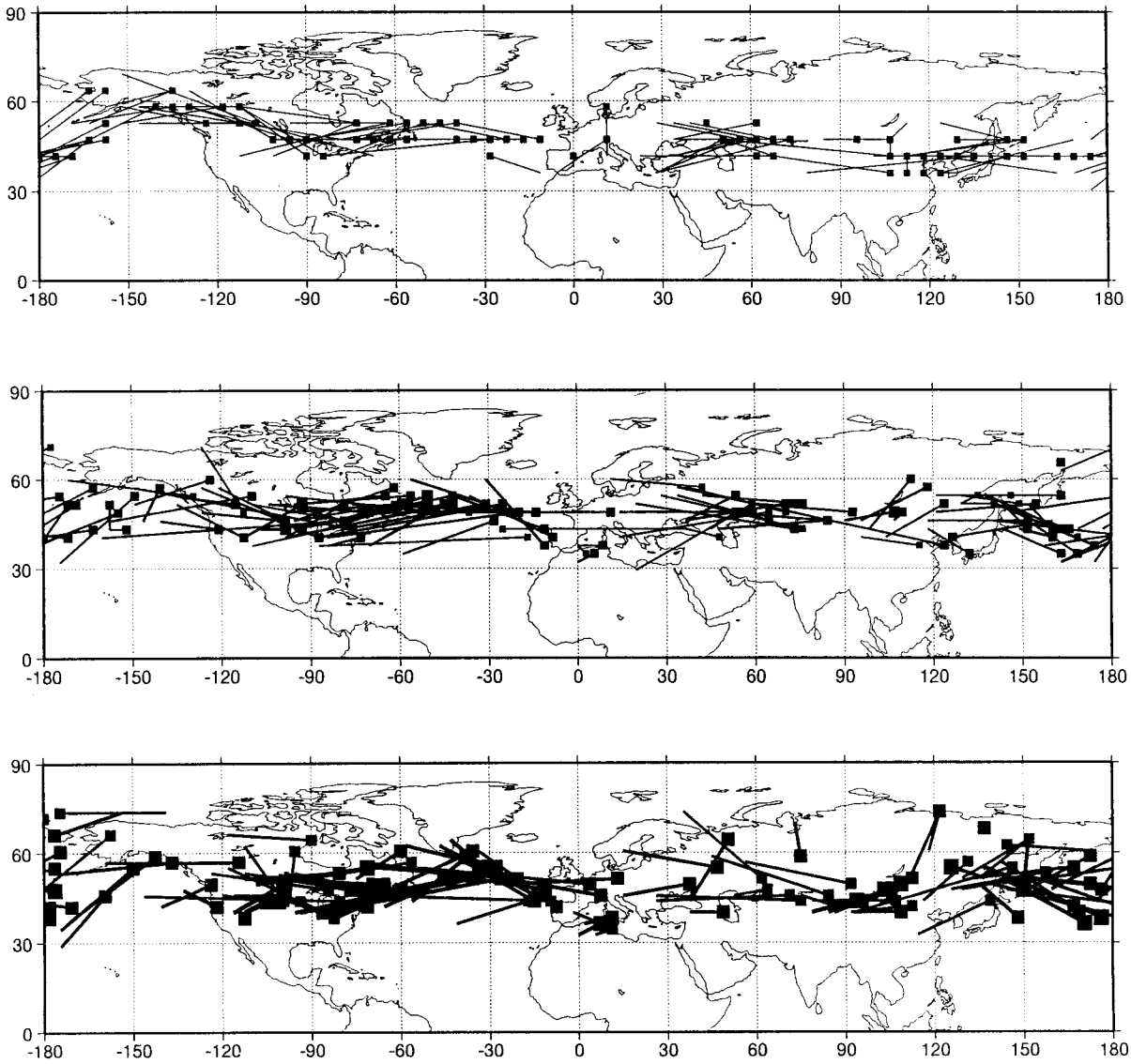

FIG. 7. Geographical distribution, based on enstrophy, of (a) T21_12, (b) T42_3, and (c) T63_3 singular vectors. For each singular vector, a square, whose size is proportional to the growth rate, identifies the position at optimization time. The position at optimization time is connected by a bar to the position at initial time.

and T63 they are 2 to 3 times smaller, not shown for reason of space). Due to the interaction of scales with total wavenumber $n \leq 21$ with scales with $n > 21$, the average similarity index computed for T42 or T63 growing subspaces is smaller than the similarity indices computed for T21 growing subspaces.

Table 4 suggests that, especially for T42 and T63 singular vectors, the similarity between growing subspaces computed for successive days is rather small. Concerning the last question, results indicate that similarity indices do depend on the resolution.

Q3. *How similar are growing subspaces generated using singular vectors computed for consecutive days and evolved to verify at the same time? More precisely, how similar are* $\mathbf{P}^{d,\mathrm{Tn}}(t)$, $\mathbf{P}^{d',\mathrm{Tn}}(t')$ *for* $d + t = d' + t'$? *Does the similarity depend on the resolution* Tn *and/or on the forecast times* t, t'?

Table 5 lists the average similarity index computed between the growing subspace of day d evolved for time t, and the growing subspace of day $d + 1$ evolved for time t', with t and t' defined so that the growing subspaces verify at the same time.

Considering growing subspaces with the same resolution (i.e., comparing values on the same row) the similarity index increases with forecast times, especially

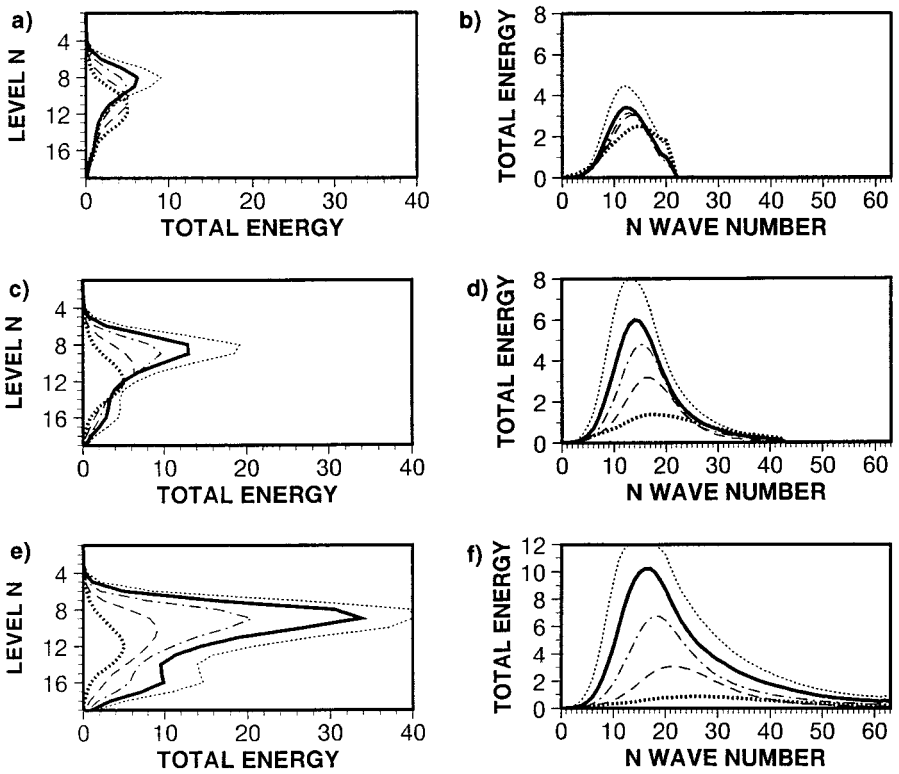

FIG. 8. Average total energy ($m^2\ s^{-2}$) (a) vertical distributions and (b) spectra of T21 singular vectors, at initial time (bold-dot, times 30), at +12 h (thin-dash, times 12), at +24 h (thin-chain-dash, times 2), at optimization time +36 h (bold-solid, times 3), and at +48 h (thin-dot, times 3). (c), (d): As (a), (b) but for T42 singular vectors. (e), (f): As (a), (b) but for T63 singular vectors. Please note that the vertical axis of panel (f) is different from the one of panels (b) and (d).

when going from (t = 24 h, t' = 0) to (t = 36 h, t' = 12 h). In fact, because of the upscale total energy transfer (Fig. 8), energy is concentrated more into larger scales at optimization rather than initial time. As already pointed out above, for each (t, t') the average similarity index decreases with singular vectors' resolution.

Generally speaking, Table 5 indicates that the similarity between growing subspaces computed for consecutive days and verifying at the same forecast time is rather poor.

d. Forecast error projection index

Figure 10 shows the daily value of the projection index $PI_N^{d,Tn}$(36 h) relative to T63 (solid), T42 (dashed), and T21 (dot) singular vectors, computed at truncation N = 21. Generally speaking, the projection indices are rather small. This can be seen as an indication that more than 10 singular vectors are needed to describe the growing part of the forecast error (one should consider that the phase space dimension at T42 with 19 vertical levels is of the order 10^5). It is worth mentioning two other effects that could contribute to this performance, the fact that the singular vectors have been computed at a resolution that is coarser than T213L31 (let us remind the reader that the forecast error is the error of the +36-h forecast given by the high-resolution T213L31 ECMWF model), and the fact that the linear tangent and adjoint model versions lack in physical parameterization.

Comparing the projection indices for the three different resolutions, T42 and T63 singular vectors are better able to capture the forecast error scales with $n \leq 21$ in eight out of 11 cases. This is true also on average (see Fig. 4a). The fact that T63 singular vectors do not outperform T42 singular vectors could indicate that the need for an inclusion of more physical processes in the tangent model versions is stronger at higher resolution.

To assess the relevance of the singular vectors of day d to describe the error of the forecast started on day d, projection indices computed using singular vectors of day d, $d - 1, \ldots, d - 8$ have been compared. For all resolutions, the average projection index computed using lagged singular vectors (Fig. 11) decreases when the time lag increases. The effect is more evident at T42 and T63 resolution because of the higher dimensionality of the system at these two resolutions.

As a further verification, forecast error has been projected onto the first 10 singular vectors of a randomly chosen date. Considering T42 resolution, the average percentage of forecast error explained by the randomly

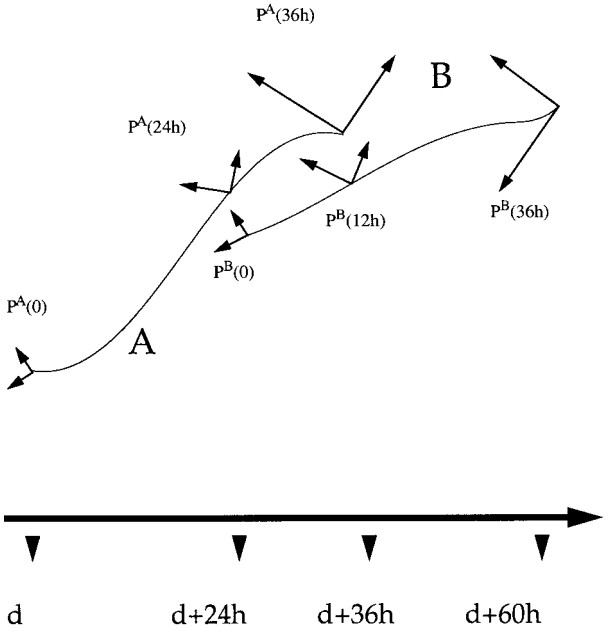

FIG. 9. Schematic of the comparison between the growing subspaces of day d computed following the trajectory **A** at forecast times $t = 24$ h, 36 h [subspaces $\mathbf{P}^{\mathbf{A}}(t = 24\text{ h})$, $\mathbf{P}^{\mathbf{A}}(t = 36\text{ h})$], and the growing subspaces of day $d + 1$, computed following the trajectory **B** at forecast times $t = 0$, 12 h [subspaces $\mathbf{P}^{\mathbf{B}}(t = 0)$, $\mathbf{P}^{\mathbf{B}}(t = 12\text{ h})$].

chosen singular vectors is 14%, compared to the value of 28% for the singular vectors of the correct day (Fig. 11).

6. Conclusions

For a period of 11 consecutive days, singular vectors have been computed at horizontal spectral triangular truncation T21, T42, and T63, with a 36-h optimization time interval, with a total energy-based scalar product, and with a ∇^4 horizontal diffusion with damping times on the smallest scale (on divergence) ranging from 1.5 to 48 h.

A metric based on total energy has been used to investigate similarity between singular vectors computed in different configurations. This metric has been defined to be total wavenumber dependent, to highlight the effect of spectral truncation on the definition of different components of the forecast states.

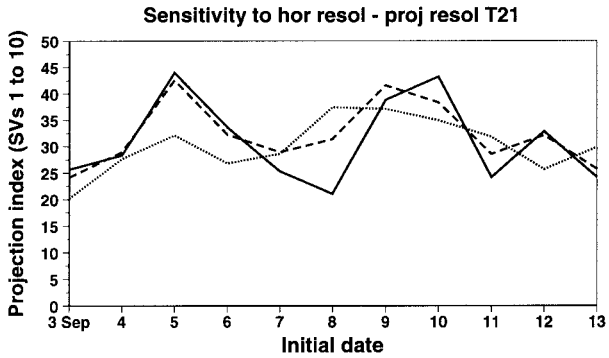

FIG. 10. Daily projection index computed considering scales with total wavenumber $0 \leq n \leq 21$ relative to T63 (solid), T42 (dashed), and T21 (dotted) singular vectors.

TABLE 3. Average similarity index (in percentage), at initial and optimization time, between T21 and T42 growing subspaces computed with a T21 norm truncation (first row), T21 and T63 growing subspaces computed with a T21 norm truncation, and T42 and T63 growing subspaces computed with a T21 and a T42 norm truncation. Standard deviations are reported in brackets.

Norm truncation:	$N = 21$		$N = 42$	
Time:	$t = 0$	$t = 36$ h	$t = 0$	$t = 36$ h
$\bar{s}[\mathbf{P}^{d,T21}(t), \mathbf{P}^{d,T42}(t); N]$	45.9 (4.7)	52.1 (7.5)	—	—
$\bar{s}[\mathbf{P}^{d,T21}(t), \mathbf{P}^{d,T63}(t); N]$	23.5 (2.6)	28.6 (5.0)	—	—
$\bar{s}[\mathbf{P}^{d,T42}(t), \mathbf{P}^{d,T63}(t); N]$	58.7 (4.3)	61.2 (3.3)	52.2 (3.6)	54.0 (3.8)

First, the effect of spectral truncation on the trajectory definition has been investigated (this is an important issue since the singular vectors are computed following a time-evolving trajectory). The comparison of T21, T42, and T63 trajectories has shown that T21 trajectories are quite different from either T42 or T63 trajectories, while these latter are much more similar. When compared to analysis fields, the error of T42 (T63) trajectories is 30% (35%) smaller than the error of T21 trajectories. In particular, the components of the analysis field with total wavenumber $n \leq 21$ are already well described by T42 trajectories. A slightly better description of the total wavenumber components $n \leq 42$ is given by T63 trajectories.

Then, at each resolution, sensitivity of singular vectors' characteristics to horizontal diffusion has been investigated. Horizontal diffusion damping times ranging from 1.5 to 48 h have been considered. It has been shown how horizontal diffusion could be used to control the singular vectors' characteristics. For each resolution, forecast error projections onto the leading 10 singular vectors have been shown to be sensitive to the choice of horizontal diffusion damping times. Results suggest that slightly better projections are obtained if a horizontal diffusion damping time on the smallest scale (on

TABLE 4. Columns 1–3: Average similarity index (in percentage) computed between the growing subspaces of consecutive days ($d' - d = 24$ h) at optimization time $t = 36$ h, at different resolutions and for different norm truncation N. Columns 4–6: As columns 1–3 but relative to the similarity index between the growing subspaces of day d and day $d + 48$ h. Standard deviations range from 4 for the smallest similarity indices to 8 for the largest ones (not reported).

Time shift $d' - d$:	24 h			48 h		
Norm truncation N:	21	42	63	21	42	63
$\bar{s}[\mathbf{P}^{d,T21}(36\text{ h}), \mathbf{P}^{d',T21}(36\text{ h}); N]$	55.5	—	—	39.4	—	—
$\bar{s}[\mathbf{P}^{d,T42}(36\text{ h}), \mathbf{P}^{d',T42}(36\text{ h}); N]$	41.7	33.4	—	24.9	19.0	—
$\bar{s}[\mathbf{P}^{d,T63}(36\text{ h}), \mathbf{P}^{d',T63}(36\text{ h}); N]$	32.0	18.5	16.1	16.8	9.3	7.9

TABLE 5. Columns 1–3: Average similarity index computed between the growing subspaces of day d evolved to time $t = 24$ h, and the growing subspace of day $d + 1$ at initial time $t' = 0$, at different resolutions and for different norm truncation N. Columns 4–6: As columns 1–3 but for the growing subspaces of day d evolved to time $t = 36$ h, and the growing subspace of day $d + 1$ evolved to time $t' = 12$ h. Columns 7–9: As columns 1–3 but for the growing subspaces of day d evolved to time $t = 48$ h, and the growing subspace of day $d + 1$ evolved to time $t' = 24$ h. Standard deviations range from 1.5 for the smallest similarity indices to 8 for the largest ones (not shown).

Forecast times: t =	24 h			36 h			48 h		
t' =	0			12 h			24 h		
Norm truncation N:	21	42	63	21	42	63	21	42	63
$\bar{s}[\mathbf{P}^{d,T21}(t), \mathbf{P}^{d+1,T21}(t'); N]$	14.5	—	—	32.9	—	—	56.9	—	—
$\bar{s}[\mathbf{P}^{d,T42}(t), \mathbf{P}^{d+1,T42}(t'); N]$	14.0	7.2	—	29.5	23.9	—	42.9	34.5	—
$\bar{s}[\mathbf{P}^{d,T63}(t), \mathbf{P}^{d+1,T63}(t'); N]$	12.5	4.5	3.2	27.4	16.0	15.0	33.1	19.1	17.0

divergence) of 12 h is used at T21, and if a 3-h damping time is used at T42 and T63.

Following these results, attention has been focused on T21, T42, and T63 singular vectors computed with, respectively, a 12-, 3-, and 3-h damping time. Singular vectors' growth (over the 36-h optimization time interval) has been shown to continue to increase with resolution, specifically by a factor of ~1.5 when going from T21 to T42 resolution, and by ~1.6 when further enhancing resolution to T63. Generally speaking, the T21, T42, and T63 geographical distributions and total energy vertical distributions have been shown to be quite similar. By contrast, differences were detected in the singular vectors' total energy spectra.

One of the points addressed by comparing T21, T42, and T63 singular vectors has been ''whether linear growth rates continue to increase with resolution, and if so, at what rate'' (Hartmann et al. 1995). Results indicate that the rate of increase of the singular vector growth when scales with total wavenumber $n > 42$ are introduced is similar to the rate of increase obtained when going from T21 to T42. The comparison of T21, T42, and T63 growing subspaces (defined using the first 10 fastest growing singular vectors) suggests that the contribution of scales with total wavenumber $n > 21$ is larger than the contribution of scales with total wavenumber $n > 42$.

Singular vectors computed for successive days have been compared with two different methods. Both methods suggest that there is poor similarity also when singular vectors are evolved for at least 12 h to be verified at the same time, especially at high resolution.

Finally, singular vectors have been compared to forecast error, to quantify the impact of horizontal resolution on the forecast error projection onto the 10 leading vectors. Results indicate that slightly higher projections can be obtained if T42 or T63 singular vectors are used. The fact that the impact of horizontal resolution is marginal, although better agreement (e.g., between forecast error and singular vectors spectra) is achieved when high resolution is used, could be because the lack of physical parametrization is more detectable at resolutions higher than T21. [In fact, as shown by Errico and Ehrendorfer (1995), the inclusion, for example, of moist processes can change the singular vectors' growth rate and structure, and although it has not been demonstrated yet, it seems reasonable to expect a stronger impact at high resolution.]

The relevance of the singular vectors of day d in describing the error of the forecast started on day d has been addressed by comparing projection indices computed using singular vectors of day d, $d - 1, \ldots, d - 8$. Results indicate that, although in absolute terms values are rather small, largest projections are achieved when the singular vectors of the correct day are used, and that projection indices decrease as the time lag increases. The fact that absolute values are small indicates that more than 10 singular vectors are needed to capture the growing components of forecast error.

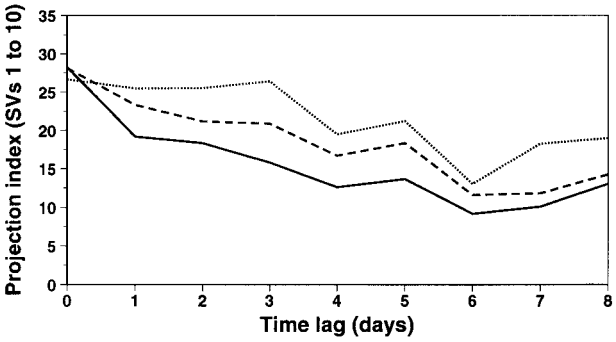

FIG. 11. Average projection index as a function of the time lag (in days) for T63 (solid), T42 (dashed), and T21 (dotted) singular vectors.

Acknowledgments. The author would like to thank Anthony Hollingsworth and Tim Palmer for very useful comments given to an early version of this manuscript, and Mariano Hortal and Clive Temperton for valuable discussions on the role of horizontal diffusion in numerical weather prediction models. The careful reviews of three anonymous referees provided helpful comments and suggestions.

REFERENCES

Borges, M. D., and D. L. Hartmann, 1992: Barotropic instability and optimal perturbations of observed non-zonal flows. *J. Atmos. Sci.,* **49,** 335–354.

Boyd, J. P., 1983: The continuous spectrum of linear Couette flow with beta effect. *J. Atmos. Sci.,* **40,** 2304–2308.

Buizza, R., 1994: Sensitivity of optimal unstable structures. *Quart. J. Roy. Meteor. Soc.,* **120,** 429–451.

——, 1995: Optimal perturbation time evolution and sensitivity of ensemble prediction to perturbation amplitude. *Quart. J. Roy. Meteor. Soc.,* **121,** 1705–1738.

——, and T. N. Palmer, 1995: The singular vector structure of the atmospheric general circulation. *J. Atmos. Sci.,* **52,** 1434–1450.

——, J. Tribbia, F. Molteni, and T. N. Palmer, 1993: Computation of optimal unstable structures for a numerical weather prediction model. *Tellus,* **45A,** 388–407.

——, R. Gelaro, F. Molteni, and T. N. Palmer, 1997: Ensemble prediction using high resolution singular vectors. *Quart. J. Roy. Meteor. Soc.,* **123,** 1007–1033.

Errico, E. R., and M. Ehrendorfer, 1995: Moist singular vectors in a primitive-equation regional model. Preprints, *10th Conf. on Atmospheric and Oceanic Waves and Stability,* Big Sky, MT, Amer. Meteor. Soc., 235–238.

Farrell, B. F., 1982: The initial growth of disturbances in a baroclinic flow. *J. Atmos. Sci.,* **39,** 1663–1686.

——, 1988a: Optimal excitation of neutral Rossby waves. *J. Atmos. Sci.,* **45,** 163–172.

——, 1988b: Optimal excitation of perturbations in viscous shear flow. *Phys. Fluids,* **31,** 2093–2101.

Hartmann, D. L., R. Buizza, and T. N. Palmer, 1995: Singular vectors: The effect of spatial scale on linear growth of disturbances. *J. Atmos. Sci.,* **52,** 3885–3894.

Lacarra, J.-F., and O. Talagrand, 1988: Short-range evolution of small perturbations in a barotropic model. *Tellus,* **17,** 321–333.

Molteni, F., and T. N. Palmer, 1993: Predictability and finite-time instability of the northern winter circulation. *Quart. J. Roy. Meteor. Soc.,* **119,** 269–298.

——, R. Buizza, T. N. Palmer, and T. Petroliagis, 1996: The ECMWF Ensemble Prediction System: Methodology and validation. *Quart. J. Roy. Meteor Soc.,* **122,** 73–119.

Noble, B., and J. W. Daniel, 1977: *Applied Linear Algebra.* Prentice-Hall, 477 pp.

Palmer, T. N., R. Gelaro, J. Barkmeijer, and R. Buizza, 1998: Singular vectors, metrics and adaptive observations. *J. Atmos. Sci.,* **55,** 633–653.

Petterssen, S., and S. J. Smebye, 1971: On the development of extratropical cyclones. *Quart. J. Roy. Meteor. Soc.,* **97,** 457–482.

Toth, Z., and E. Kalnay, 1993: Ensemble forecasting at NMC: The generation of perturbations. *Bull. Amer. Meteor. Soc.,* **74,** 2317–2330.

Zeng, Q.-C., 1983: The evolution of a Rossby-wave packet in a three dimensional baroclinic atmosphere. *J. Atmos. Sci.,* **40,** 73–84.